24th COBEM - 2017

24th ABCM International Congress of Mechanical Engineering
December 3-8, 2017, Curitiba, PR, Brazil

COBEM-2017-0514
STUDY OF VISCOUS FLOWS USING HIGH-ORDER METHODS AND CURVED BOUNDARY TREATMENT

André Ribeiro de Barros Aguiar
Fábio Mallaco Moreira
Eduardo Jourdan
Instituto Tecnológico de Aeronáutica, DCTA/ITA, São José dos Campos, SP, 12228-900, Brazil
ufabc.andre@gmail.com, fabiom91@gmail.com, eduardojourdan92@gmail.com

João Luiz F. Azevedo
Instituto de Aeronáutica e Espaço, DCTA/IAE/ALA, São José dos Campos, SP, 12228-904, Brazil
joaoluiz.azevedo@gmail.com

Abstract: *In the context of compact high-order numerical schemes in Computational Fluid Dynamics (CFD), a meaningfully accurate solution can only be obtained if a corresponding high-order curved representation of the true geometrical boundaries is used. An* a posteriori *approach is used in the present work in order to generate a curved mesh conformed to the surface of the model,* i.e.*, given a common flat sided mesh and a Computer Aided Design (CAD) representation of the geometry, it is possible to generate the curved boundary representation. This approach, however, leads to the presence of invalid cells when highly stretched boundary layer meshes have to be represented. In order to overcome this problem, a moving mesh technique based on the Radial Basis Function (RBF) strategy is employed and results of the capabilities of these solutions are shown for aerospace-like applications.*
Keywords: *Unstructured High-Order Meshes, Curved Boundaries, Radial Basis Function, Moving Meshes, CFD*

1 INTRODUCTION

Computational Fluid Dynamics (CFD) methods currently being used for industrial applications are mainly 2nd-order accurate and have achieved an acceptable level of robustness for everyday deployment in aeronautical engineering scenarios. In recent years, however, the requirements of tackling problems with higher accuracy have motivated the use of high-order methods for CFD, specially for vortex dominated or aeroacoustic simulations. Moreover, high-order methods offer the possibility of reducing simulation costs for given solution accuracy levels, when compared to low-order schemes.

It was observed that the accuracy and efficiency on the order of convergence of these compact high-order methods is negatively affected by an unsuitable representation of the physical geometrical boundaries (Bassi and Rebay, 1997a). Therefore, as an effort to fully benefit from the advantages of high-order methods, meshes should also be constructed within a high-order approximation of the geometry. This leads to a curved mesh representation, which reportedly decreases the entropy generated near walls (Aguiar *et al.*, 2016; Gao *et al.*, 2010) and, hence, removes undesirable oscillatory results. In addition, the same literature results have demonstrated that even a fine grid is not able to properly handle the problem and oscillations may still appear.

The generation of high-order meshes which conform to the boundary geometry is still not a well resolved issue. For the case of large isotropic cells, the resulting curved mesh is often satisfactory when only faces that are in contact with the boundary are curved. However, when highly anisotropic cells are necessary, which is often the case for boundary layers, this strategy may lead to auto-intersecting and, hence, invalid cells with negative areas. It is necessary, then, to come up with a strategy to propagate the boundary deformation into the interior of the mesh.

Previous work in this field proposes different mesh techniques to identify mesh entities that produce invalid elements and eliminate the problems via node repositioning and edge swapping (Luo *et al.*, 2004) or via a hybrid meshing strategy in such a way that prism elements are used close to the curved boundary where a curvature based refinement is considered (Sherwin and Peiró, 2002). A recent study from Persson and Peraire (2009) proposes a different approach based on an elastic analogy as an effort to avoid invalid elements. Specifically, they propose to model the geometry of the domain as an elastic solid so that external loadings are obtained when prescribing the boundary displacement. As a result, an equilibrium equation can be solved to find the correct positioning of interior nodes in a way that no invalid elements are generated.

The present work proposes another approach to regularly deform the interior mesh whenever a curved geometrical boundary is required in such a way that no invalid elements are allowed. The main contribution of the present work

consists of adopting a fairly established moving mesh technique to resolve the issues with invalid elements. A radial basis function (RBF) interpolation (Buhmann, 1993) is used as a moving mesh technique so as to provide node movement for all interior mesh nodes given a prescribed movement of some boundary nodes, hence, providing a fully valid high-order mesh. Furthermore, mesh movement capabilities are demonstrated for aeronautical configurations.

The methodology is described in Sections 2, 3 and 4, whereas examples of successfully generated curved meshes considering highly curved boundaries and anisotropic cells are shown as a result of the present work in Section 5. Furthermore, different mesh movements and their characteristics are discussed for the extension of the RBF applications.

2 NAVIER-STOKES FORMULATION

The flows of interest in the present work are assumed to be adequately modeled by the 2-D Navier- Stokes equations. They are formed by the combination of three conservation laws, namely the conservation of mass, the momentum equations and conservation of energy, that are combined with the equation of state for perfect gases to form a closed system taking into account viscous effects and heat conduction in the fluid. These equations can be written in differential form as

$$\frac{\partial Q}{\partial t} + \frac{\partial (E_e - E_v)}{\partial x} + \frac{\partial (F_e - F_v)}{\partial y} = 0\,. \tag{1}$$

The vector of conserved variables, Q, and the convective flux vectors, E_e and F_e, are given in terms of velocities in x and y direction (u and v), density (ρ), pressure (p) and total energy per unit volume (ε), by

$$Q = \left\{ \begin{array}{c} \rho \\ \rho u \\ \rho v \\ \varepsilon \end{array} \right\}, \qquad E_e = \left\{ \begin{array}{c} \rho u \\ \rho u^2 + p \\ \rho uv \\ (\varepsilon + p)u \end{array} \right\}, \qquad F_e = \left\{ \begin{array}{c} \rho v \\ \rho uv \\ \rho v^2 + p \\ (\varepsilon + p)v \end{array} \right\}. \tag{2}$$

The aforementioned equation of state for perfect gases can be written as

$$p = (\gamma - 1)\left[\varepsilon - \frac{1}{2}\rho(u^2 + v^2)\right], \tag{3}$$

where the ratio of specific heats, γ, is set as 1.4 for all computations in this work.

The viscous flux vectors are defined as

$$\begin{aligned} E_v &= \mu \left\{ \begin{array}{c} 0 \\ 2u_x + \lambda(u_x + v_y) \\ v_x + u_y \\ u[2u_x + \lambda(u_x + v_y)] + v(v_x + u_y) + \frac{C_p}{Pr} T_x \end{array} \right\}, \\ F_v &= \mu \left\{ \begin{array}{c} 0 \\ v_x + u_y \\ 2v_y + \lambda(u_x + v_y) \\ v[2v_y + \lambda(u_x + v_y)] + u(v_x + u_y) + \frac{C_p}{Pr} T_y \end{array} \right\}, \end{aligned} \tag{4}$$

where μ is the dynamic viscosity coefficient, C_p is the specific heat at constant pressure and Pr stands for the Prandtl number of the fluid. T is the local temperature of the flow and λ is defined as $-2/3$, following the Stokes hypothesis.

The discretization and solution procedure chosen to test the results was the high-order Spectral Difference (SD) formulation due Wang and Liu (2002), which properly handles quadrilateral elements in a finite difference-like manner and, hence, is suitable for viscous simulation. The SD method employs a finite difference-like scheme and, in order to achieve an efficient implementation, all cells in the physical domain, (x, y), are transformed into a unit square element in the computational domain as observed in Fig. 1. This step is specially important since transformation is more efficiently represented near boundaries when curved edges are assigned.

Usually, metric terms and the Jacobian matrix of the transformation can be computed in a pre-processing step and kept in memory for stationary problems. However, further implementations considering unsteady aerodynamics will require metric terms to be recalculated every time step. The implementation follows the formulation presented in Wang *et al.* (2007) and May and Jameson (2006). The governing equations in the physical domain are transformed into the computation domain, and are rewritten as

$$\frac{\partial \widetilde{Q}}{\partial t} + \frac{\partial (\widetilde{E_e} - \widetilde{E_v})}{\partial \xi} + \frac{\partial (\widetilde{F_e} - \widetilde{F_v})}{\partial \eta} = 0\,, \tag{5}$$

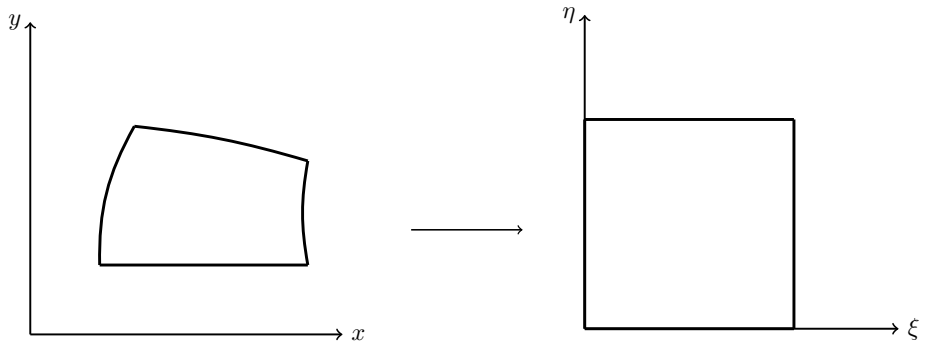

(a) Physical Element (c) Standard Element.

Figure 1: Transformation from physical domain (x,y) to computational domain (ξ,η).

where $\widetilde{Q} = |J|\, Q$ and J is the Jacobian matrix of the coordinate transformation, given by

$$J = \begin{pmatrix} x_\xi & x_\eta \\ y_\xi & y_\eta \end{pmatrix} . \tag{6}$$

The fluxes and conservative variables are, then, stored in the standard element as per the SD formulation following the procedures described in Wang and Liu (2002) and Moreira *et al.* (2015, 2016).

3 HIGH-ORDER BOUNDARY TREATMENT

In order to render the high-order reconstruction process manageable,it is of great importance to consider curved meshes which better represent more complex geometries. This has the side effect of reducing the required number of cells in the domain. Furthermore, the use of lower-order approximations of a curved boundary leads to imprecise solutions when using compact high-order schemes, as observed by Bassi and Rebay (1997b). Therefore, it is mandatory to use a precise description of the curved geometry of the boundary so as to obtain meaningful and accurate results.

An *a posteriori* approach was used to render the high-order mesh in the present work, i.e., after a usual flat sided mesh was generated, it could be compared to a geometry description in which new nodes were projected, as can be seen in Fig. 2. This strategy is considered overcomes some of the obstacles of directly generating a high-order mesh whilst taking advantage of the robustness of current linear mesh generators (Wang *et al.*, 2013; Peiró *et al.*, 2013).

The usual geometry entity used to describe 2 dimensional configurations is the Non-Uniform Rational B-Spline (NURBS) curve. The process of curving a mesh considering the NURBS curve exploits the advantage of projecting the nodes onto the true boundary. The procedures undertaken to reconstruct the NURBS curve and correctly project the nodes are detailed in Aguiar *et al.* (2016). Figure 2 gives an example of the projection step for a second order quadrangular cell.

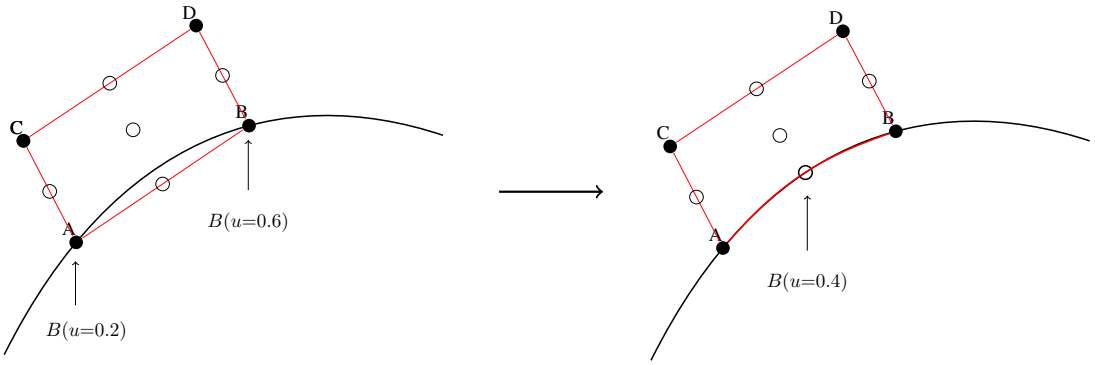

Figure 2: Node projection step onto the B-spline

Often, the concern of viscous flows is the analysis of properties inside a thin boundary layer. The dimension of a boundary layer is excessively small when compared to the dimension of the model and, more importantly, huge gradients are observed within it, which suggests that the mesh near this region ought to be well refined in order to capture acceptable results. Moreover, the higher the Reynolds number, the more prohibitive will be the mesh capable of capturing reasonable results. The higher-order meshes, in this sense, may bring the advantage of properly representing the boundary, thus,

reducing the number of required elements to obtain the same results. It is crucial to understand that these aspects have to be considered so as to generate a reliable and robust curved mesh.

Still within the context of a solution inside a boundary layer, a problem concerning the transformation of a linear to a curved mesh known as "element inversion" needs to be highlighted. This problem comes from the fact that the properties inside a boundary layer mostly vary on the direction orthogonal to the solid boundary, which allows the mesh to be relatively less refined in the direction tangent to the boundary. In short, cells that are capable of capturing properties inside the boundary layer have, in general, a high aspect ratio which, in turn, renders those cells highly anisotropic. In the case of overly flattened cells, it is possible for the geometry to cross several cells at once and, in an attempt to curve only the cells at the boundary, the curved edge may intersect with other edges (Persson and Peraire, 2009). Numerically, element inversion is translated to a negative area - or volume, in 3-D -, which directly affects the calculation of the jacobians and, consequently, spoils the solution. Figure 3 shows a case of a highly stretched quadrilateral cell fitted to a highly curved boundary which leads to an invalid cell.

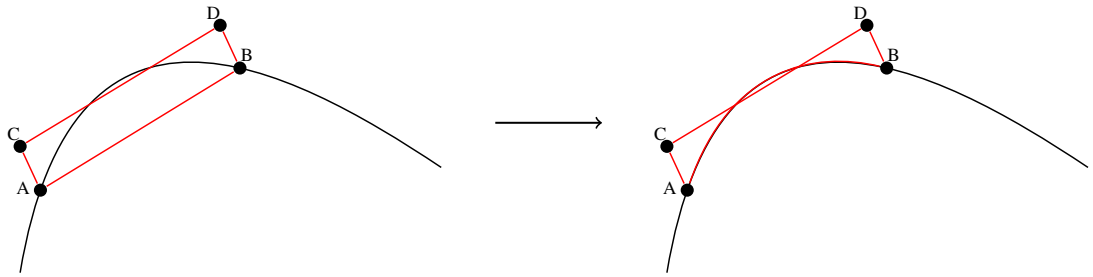

Figure 3: Mapping of a non-valid curved element.

4 RADIAL BASIS FUNCTION FORMULATION

For typical viscous aerospace problems, the gradients observed near the wall requires the mesh to be highly stretched normal to the configuration. The process of curving the boundaries described in Sec. 3, in this case, generally generates problems of cells crossing each other as previously discussed. The problem is that the curvature is being applied exclusively to edges fit to the boundary. The idea is to use Radial Basis Functions (RBF) to propagate this curvature into the interior edges of the domain.

RBFs are used to provide node movement for all mesh nodes given a prescribed movement of some boundary nodes. The displacement of all mesh nodes that have no predetermined movement is obtained by a sum of basis functions that depends on the Euclidean distance between nodes that have prescribed movement and the interior nodes of the mesh. The new displaced mesh is obtained in such a way that its topology is preserved.

The main idea behind the RBF strategy is to obtain an optimized position for the interior nodes, given a set of displacements. Two sets of nodes are important to formulate this strategy, namely $\mathbf{x}_f$ and $\mathbf{x}_m$. The subscript f represents nodes that are fixed, i.e., that does not have a prescribed movement and will soon change its position. These are the nodes whose displacements are being solved for. The subscript m represents nodes that have a prescribed movement, which, in this case, are mainly the high-order nodes projected onto the geometry boundary. It is relevant to notice that external boundaries or farfield are also considered nodes with prescribed movement ($\mathbf{x}_m$) since they have to stay still and, hence, their prescribed displacement are zero.

The formulation in Rendall and Allen (2008) leads to the definition of a coupling matrix $\mathbf{H}$ that obtains the displacement of interior nodes based on the set of prescribed movements.

$$\mathbf{u}_m = \mathbf{H} \cdot \mathbf{u}_f \tag{7}$$

where $\mathbf{u}_m$ is the vector of the new desired displacements whereas $\mathbf{u}_f$ is the vector containing the prescribed node displacements. Also, $\mathbf{H}$ is defined as:

$$\mathbf{H} = \mathbf{A}_{mf}\mathbf{C}_{ff}^{-1} \tag{8}$$

The matrices that are used to compose **H** can be written as (Rendall and Allen, 2008):

$$\mathbf{C}_{ff} = \begin{bmatrix} 0 & 0 & 0 & 1 & 1 & \dots & 1 \\ 0 & 0 & 0 & x_{f_1} & x_{f_2} & \dots & x_{f_{N_f}} \\ 0 & 0 & 0 & y_{f_1} & y_{f_2} & \dots & y_{f_{N_f}} \\ 1 & x_{f_1} & y_{f_1} & \phi_{f_1 f_1} & \phi_{f_1 f_2} & \dots & \phi_{f_1 f_{N_f}} \\ \vdots & \vdots & \vdots & \vdots & \vdots & \ddots & \vdots \\ 1 & x_{f_{N_f}} & y_{f_{N_f}} & \phi_{f_{N_f} f_1} & \phi_{f_{N_f} f_2} & \dots & \phi_{f_{N_f} f_{N_f}} \end{bmatrix} \tag{9}$$

where $\phi_{f_i f_j} = \phi(\|\mathbf{x}_{f_i} - \mathbf{x}_{f_j}\|)$ represents the radial basis functions which depends on a distance value $r = \|\mathbf{x}_{f_i} - \mathbf{x}_{f_j}\|$ considering only combinations of fixed nodes whose displacements are to be calculated. For the results further presented, a Gaussian basis function was used, such that:

$$\phi_{f_i f_j} = e^{-r^2} \tag{10}$$

and, lastly,

$$\mathbf{A}_{mf} = \begin{bmatrix} 1 & x_{m_1} & y_{m_1} & \phi_{m_1 f_1} & \phi_{m_1 f_2} & \dots & \phi_{m_1 f_{N_f}} \\ \vdots & \vdots & \vdots & \vdots & \vdots & \ddots & \vdots \\ 1 & x_{m_{N_m}} & y_{m_{N_m}} & \phi_{m_{N_m} f_1} & \phi_{m_{N_m} f_2} & \dots & \phi_{m_{N_m} f_{N_f}} \end{bmatrix} \tag{11}$$

where N_m and N_f are, respectively, the number of nodes with prescribed movement and the number of nodes that are fixed, for which the displacements are being solved.

Note that it is interesting to store the matrix $\mathbf{C}_{ff}^{-1}$ since it only depends on fixed nodes and, hence, it will remain constant throughout the problem. On the other hand, the matrix $\mathbf{A}_{mf}$ depends on the prescriptively moved nodes and, hence, has to be updated every time that movement is needed. At first glance, these properties may seem unimportant for a mesh treatment technique that consists of one single step, however, these are useful for unsteady applications where successive mesh movements are required.

5 RESULTS

5.1 Cylinder Test Case

The first result detailed in the present work considers a simple coarse mesh around a 2-D cylinder. It is a validation purpose only mesh carefully designed in such a way that only one layer of cells are allowed to be invalid. In this case, it can be observed in Fig. 4(a) that two cells are inverted such that auto-intersecting edges may be perceived. Although without auto-intersecting edges, most of the other cells close to the boundary are also invalid since the central node is inside the geometry. The application of the RBF technique uses the displacement of the projection step of the high-order nodes to generate a regular deformation of the interior mesh in such a way that it produces the desired valid cell configuration as observed in Fig. 4(b)

5.2 RAE 2822 Test Case

A more aeronautical-like application, however, can be reasoned from the RAE 2822 airfoil. A more common situation in a daily simulation is to have highly stretched anisotropic meshes that, when curved, surpasses more than one single layer of cells in order to correctly account for the boundary layer description. Generally, when trying to simulate increasingly higher Reynolds number, this restriction gets even higher. In the case observed in Fig. 5(a), it possible to notice the presence of a highly curved geometry along with highly stretched cells, which, in turn, leads to 4 or more inverted cells near the trailing edge. The application of the RBF technique, however, was capable of taking that deformation into account and accommodate the adjacent nodes to a well suited position as can be observed in Fig. 5(b), where no invalid cells are obtained.

Another problem concerning the curving strategy is that it leads to highly improper cells whenever a concave geometry needs to be curved. As opposed to the leading edge of the airfoil, in which cells are made invalid due to auto-intersecting problems, this situation leads to widely large cells that are not suitable for finite difference calculations, specially for boundary the layer. An example of such a feature is observed on the trailing edge of the RAE 2822 in Fig. 6(a), in which the geometry curves into the model. The RBF technique effectively handles this situation by homogeneously conforming these cells inward as well, as observed in Fig. 6(b).

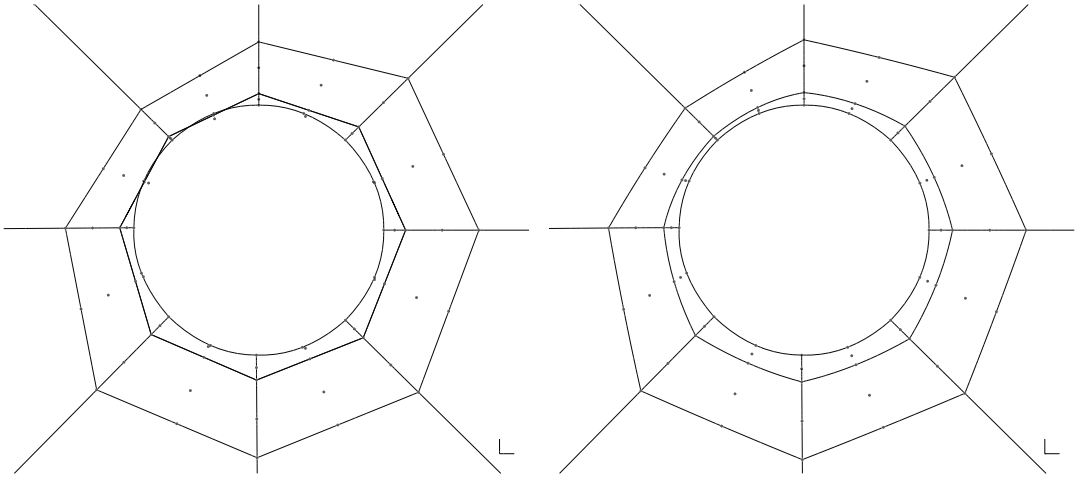

(a) Cylinder mesh with auto-intersecting cells. (b) Cylinder mesh correct via RBF.

Figure 4: RBF approach to avoid invalid cells by moving interior nodes accordingly.

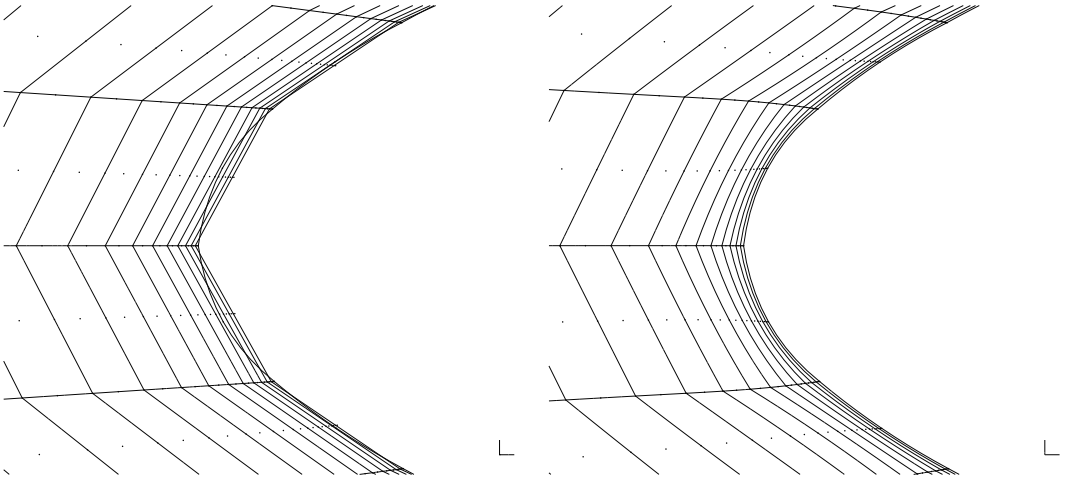

(a) RAE 2822 leading edge with invalid cells. (b) RAE 2822 leading edge corrected via RBF.

Figure 5: Anisotropic curved mesh generation and treatment via RBF.

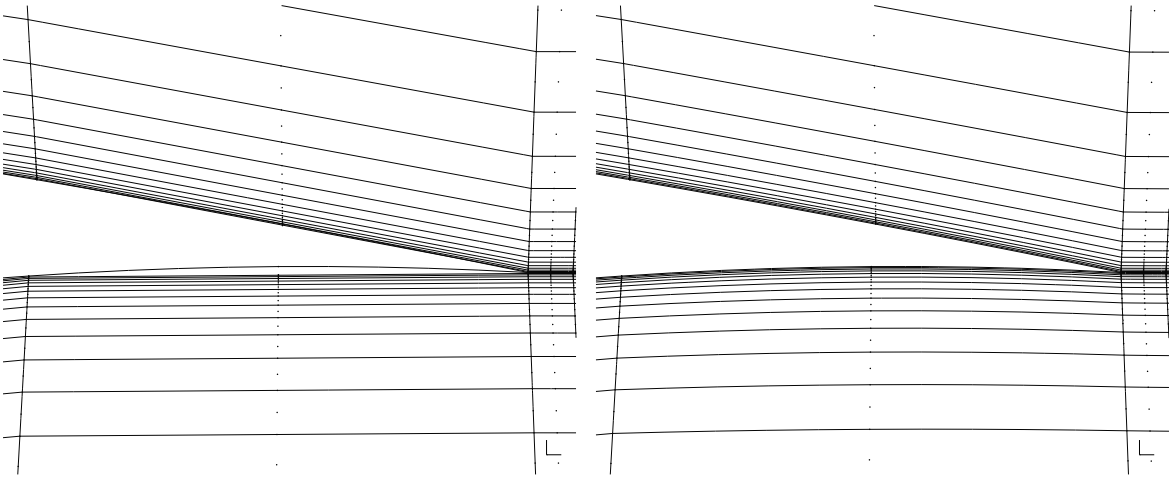

(a) RAE 2822 trailing edge with improper cells. (b) RAE 2822 trailing edge corrected via RBF.

Figure 6: Improper cells handled via RBF.

5.3 Viscous Flow Simulation

A result considering a viscous flow around a NACA 0012 airfoil is tested to validate the results obtained from the previous methodology. An unstructured mesh composed by quadrilaterals was used to represent the airfoil, as observed

in Fig. 7.

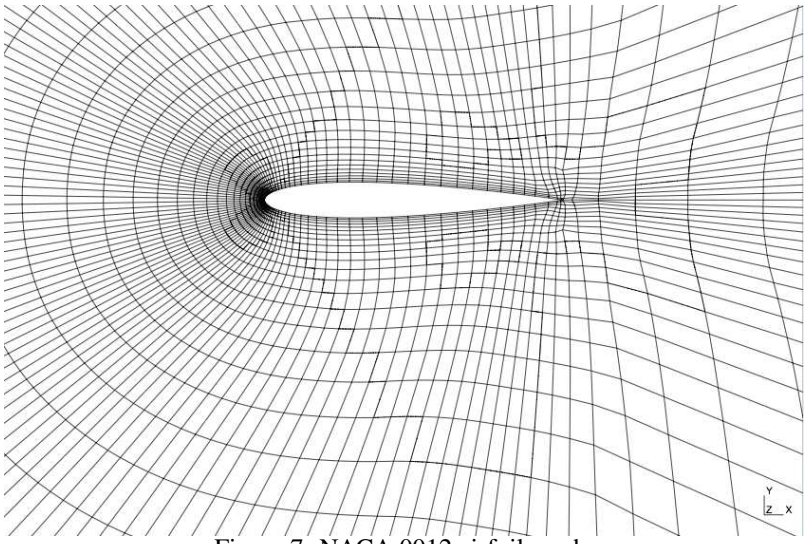

Figure 7: NACA 0012 airfoil mesh.

The flow solution is performed at Mach number 0.6 and Reynolds number 1000, for an angle of attack of $\alpha = 0°$. The contour solution at Figs. 8(a) and 8(b) shows that the results obtained correctly represents the expected behavior for a viscous flow field over a NACA 0012, which is the development of a boundary layer around the airfoil followed by a wake behind it. Figure 8 shows the results obtained for this flow condition for a third order (P2) method with both a linear and a second order mesh.

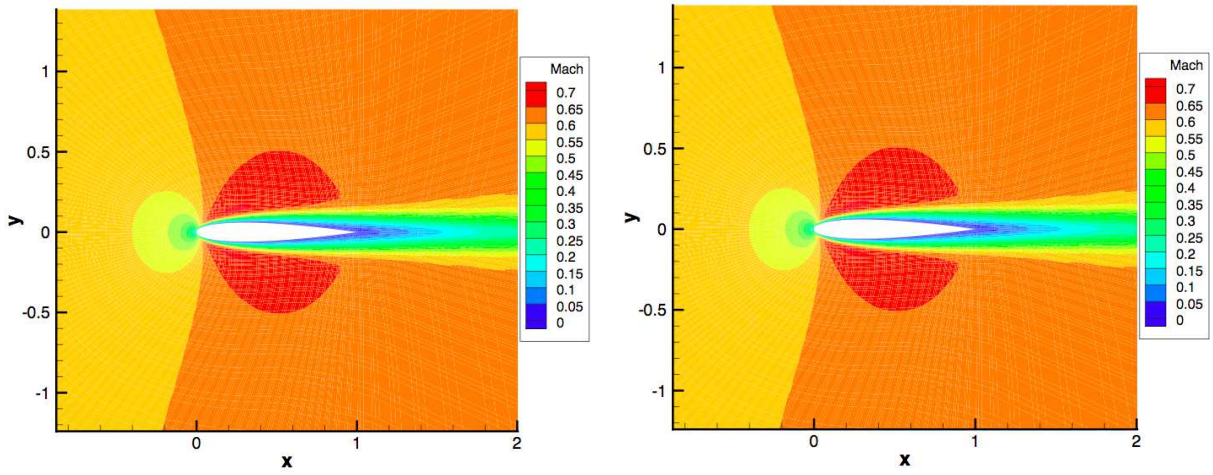

(a) Linear mesh results

(b) Second order mesh results.

Figure 8: Mach contours for a P2 spectral difference solution over a NACA 0012 airfoil.

Although the results for the Mach number field seem similar, the results presented on Figs. 9(a) and 9(b) show different patterns observed for comparisons of pressure coefficients around the airfoil wall for both upper and lower surface of the NACA0012. Results for a third order (P2) method considering both linear (Q1) and quadratic (Q2) meshes are shown. The results demonstrate the effectiveness of high-order meshes. It is interesting to notice that the curved mesh completely cancel out the oscillations present on the linear mesh results. Also, although a small asymmetry between upper and lower surfaces are expected on unstructured meshes, the results for the curved mesh enhances the symmetry.

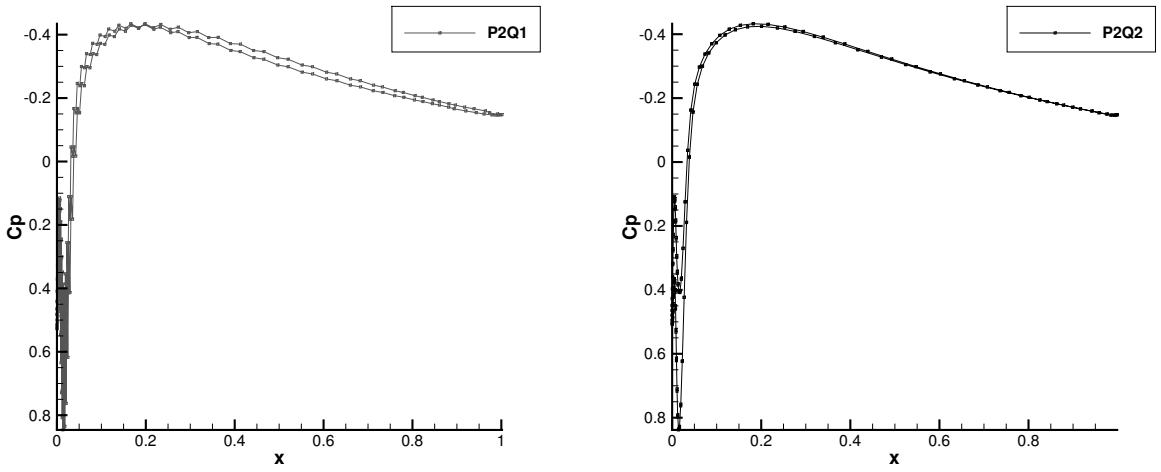

(a) Linear mesh results

(b) Second order mesh results.

Figure 9: Pressure coefficient results for second order method using linear and curved meshes.

5.4 Large Mesh Movements

Another test case considered in the present work is to apply the knowledge obtained with the RBF technique to a broader approach of moving meshes. Moving mesh is needed whenever unsteady aerodynamics are necessary. The same strategy can be applied to complex mesh movements. Figure 10 demonstrates the torsion of a cylinder by an angle of $\theta = 90°$. The result for the cylinder is obtained in one single rotation.

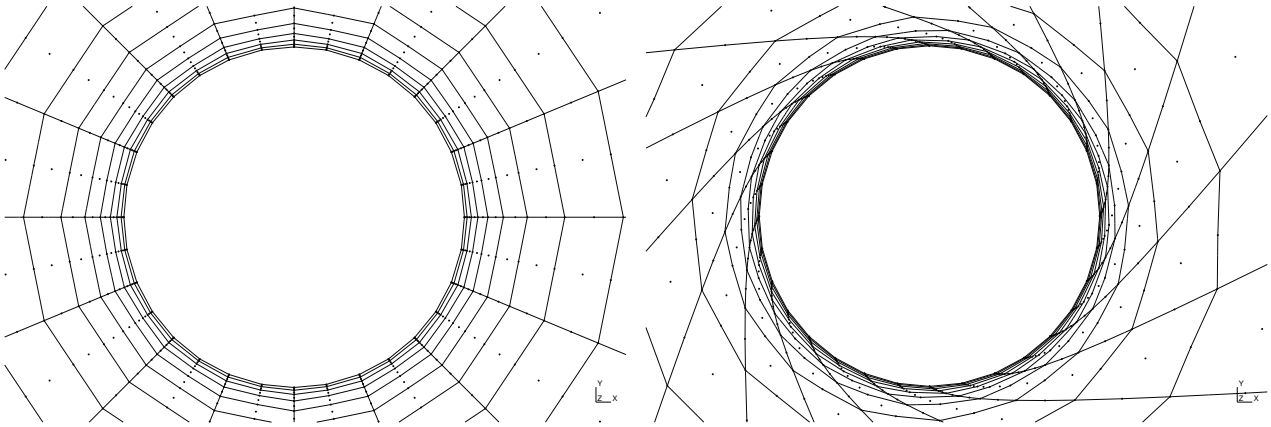

(a) Cylinder mesh.

(b) Cylinder mesh rotated by 90°.

Figure 10: Mesh movement via RBF for the cylinder mesh.

Some aeronautical applications may require a substantial displacement of the mesh. In the case of a flapping flight, for instance, the angle of attack may vary significantly. Also, simulations of turbomachinery airfoils may require such a high angle of attack. An interesting result observed is the fact that large displacements may lead to invalid mesh results if performed in one single step. Figure 11(a) shows a RAE 2822 airfoil rotated from rest to $\theta = 80°$ in one single step and Fig. 11(c) shows that edges are inadequately intersecting each other, which leads to an invalid mesh. However, if smaller substeps are taken in order to accomplish the desired final configuration, a smooth resulting mesh is observed. Figure 11(b) shows the same rotation done in two steps, *i.e.*, twice $\theta = 40°$, which leads to a valid trailing edge configuration as shown in Fig. 11(d).

5.4.1 Heaving and Pitching Airfoil Movement

Unsteady aerodynamic simulations can be performed with such capability and some test cases are the subject of future efforts of development. A test case that considers a heaving and pitching airfoil is described on the 4th International Workshop on High-Order CFD Methods (Wang *et al.*, 2015). This problem is used to test the accuracy and performance of high-order flow solver for problems with deforming domains and, hence, it is suitable to validate the contributions of

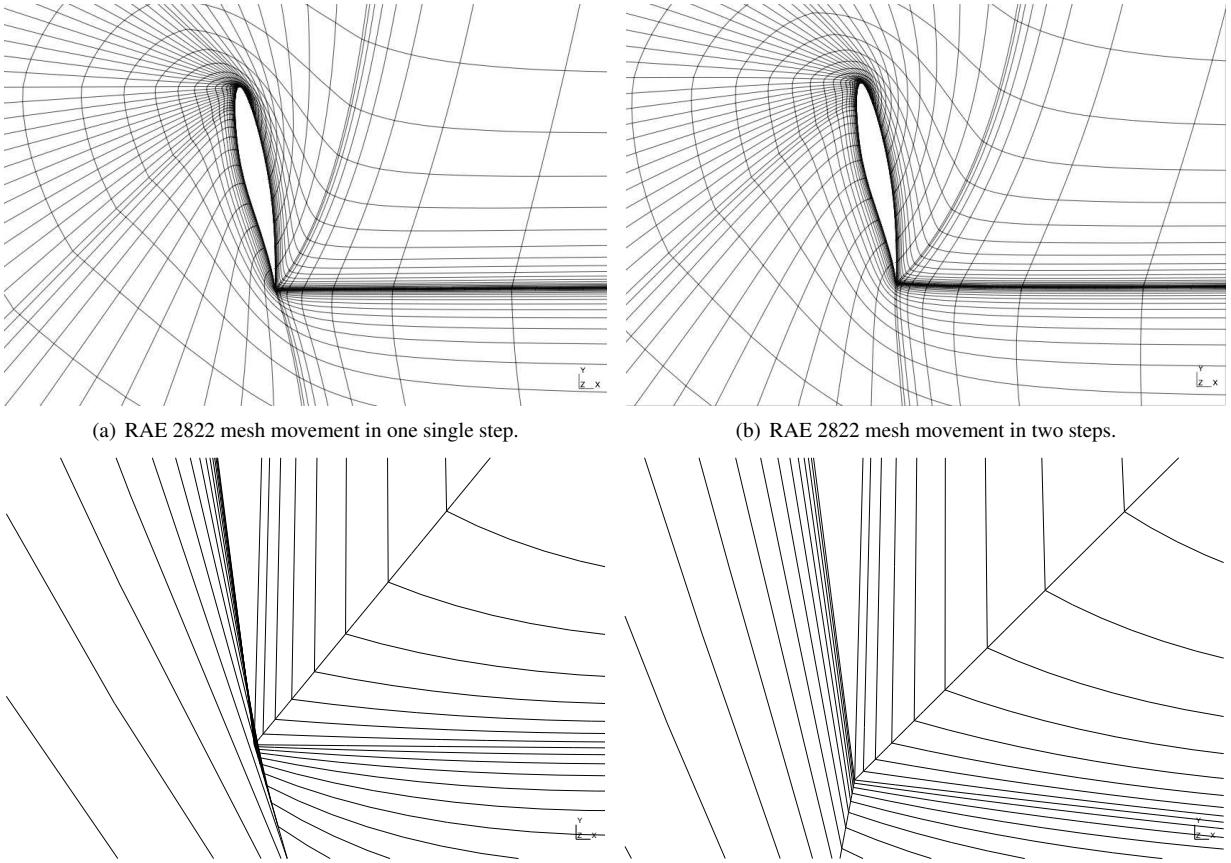

(a) RAE 2822 mesh movement in one single step.

(b) RAE 2822 mesh movement in two steps.

(c) RAE 2822 invalid trailing edge generated from one single step.

(d) RAE 2822 valid trailing edge generated from two steps.

Figure 11: Mesh movement via RBF for the RAE 2822 mesh.

the present work. Specifically, the test consists of a NACA 0012 airfoil undergoing a smooth flapping-type motion along with a vertical displacement from rest up to a position one chord length higher. The upward motion is deployed for the duration of t = 2 time units, by heaving and pitching the airfoil about a point located at the airfoil $1/3$ chord location as depicted in Fig. 12

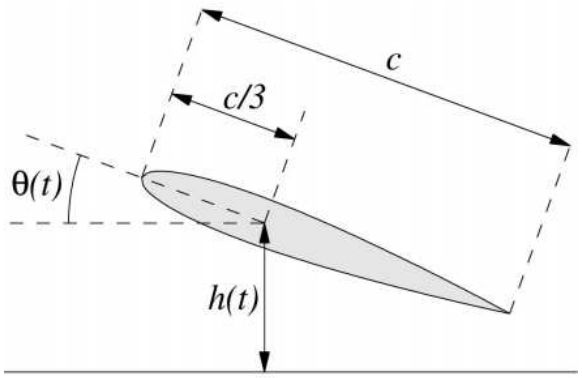

Figure 12: Airfoil configuration for motion.

The motion description is described in Table 1

Table 1: Motion description for the pitching and heaving airfoil

Case 1 - Pure heaving	**Case 2 - Flow aligning**	**Case 3 - Energy extraction**
h(t) = b_2(t)	h(t) = b_2(t)	h(t) = b_3(t)
$\theta(t) = 0$	$\theta(t)$= $A_2 \cdot b_1$(t)	$\theta(t)$= $A_3 \cdot b_1$(t)

where $A_2 = 60\pi/180$ and $A_3 = 80\pi/180$. And the motion is described within the variables

$$b_1 = t^2(t^2 - 4t + 4) \tag{12}$$

$$b_2 = t^2\frac{(3-t)}{4} \tag{13}$$

$$b_3 = t^3\frac{(-8t^3 + 51t^2 - 111t + 84)}{16} \tag{14}$$

where h(t) resembles the vertical displacement whereas $\theta(t)$ represents the pitching angle.

When $t = 1$, b_1, the variable responsible for the angular displacement is $b_1 = 1$ and, when $t = 2$, $b_1 = 0$. This means that the excursion of the airfoil starts at 0° turning up to $A_2 = 60^\circ$ or $A_3 = 80^\circ$ and return to 0°. The heaving, though, is a single movement growing monotonically from 0 to 1 distance unit for cases 1 and 2 while b_3, for the last case, ranges from 0 to 1 in a non-monotonically manner.

The mesh movement results of interest of the NACA 0012 are presented in Fig. 13. Figure 13(a) shows the NACA 0012 at its initial configuration whereas Fig. 13(b) represents the mesh at time t=1 time units for the excursion previously described of Case 3, *i.e.*, for an angle of attack $\theta = 80^\circ$.

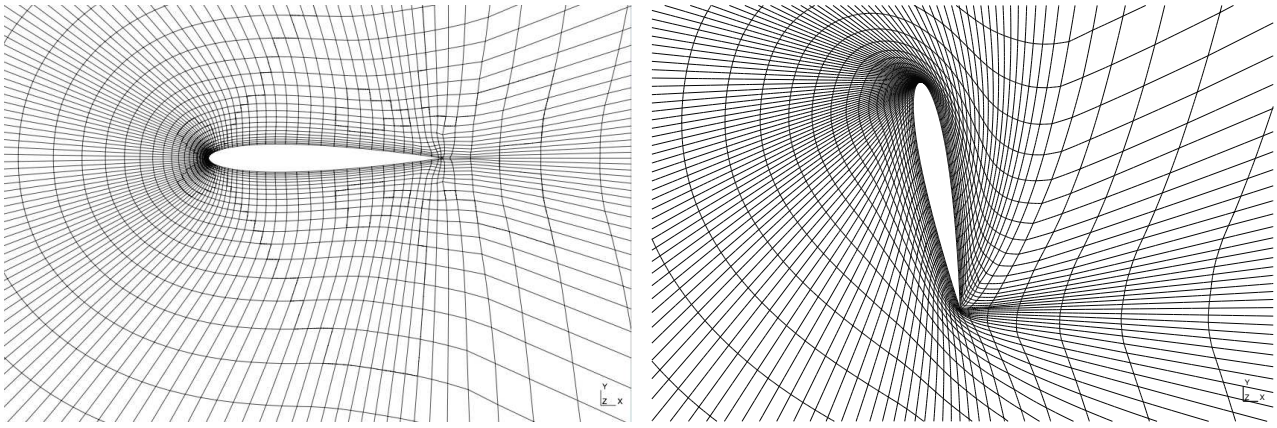

(a) NACA 0012 mesh. (b) NACA 0012 mesh rotated by 80°.

Figure 13: Mesh movement via RBF for the NACA 0012 mesh.

For this case, the mesh experiences a severe deformation, however, it is possible to observe in Fig. 14 that the mesh is still valid in the sense that there are no intersecting edges at the most problematic locations, *i.e.*, at the trailing and leading edge of the airfoil.

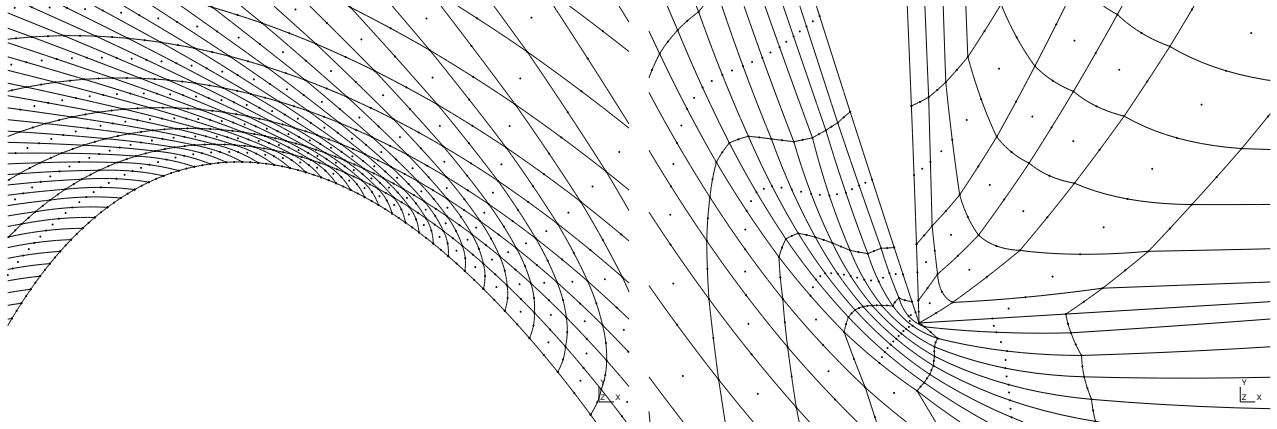

(a) NACA 0012 leading edge close-up (b) NACA 0012 trailing edge close-up.

Figure 14: Assessment of cell validity.

6 CONCLUDING REMARKS

The results obtained so far have demonstrated the capability of the RBF technique to properly handle tangled and improper cells near the boundary when a curving strategy is applied to the mesh. Furthermore, Navier-Stokes simulations

were carried out with appropriate curved meshes and comparison with their low order mesh counterparts has demonstrated the effectiveness of high-order meshes for viscous flows. Moreover, the RBF technique proved itself capable of handling the desired unsteady airfoil motion.

7 ACKNOWLEDGMENTS

The authors gratefully acknowledge the support for the present research provided by Conselho Nacional de Desenvolvimento Científico e Tecnológico, CNPq, under the Research Grants No. 309985/2013-7, No. 400844/2014-1 and No. 443839/2014-0. The work is also supported by Fundação de Amparo à Pesquisa do Estado de São Paulo, FAPESP, under Research Grant No. 2013/07375-0. The support provided by Fundação Coordenação de Aperfeiçoamento de Pessoal de Nível Superior, CAPES, through graduate scholarships for the first three authors, is also greatly appreciated.

8 REFERENCES

Aguiar, A.R.B., Moreira, F.M., , Breviglieri, E.J.C. and Azevedo, J.L.F., 2016. "High-order boundary treatment for high-order methods in computational fluid dynamics". In *Proceedings of the 16th Brazilian Congress of Thermal Sciences and Engineering*. Vitória, ES, Brazil.

Bassi, F. and Rebay, S., 1997a. "A high-order accurate discontinuous finite element method for the numerical solution of the compressible Navier-Stokes equations". *Journal of Computational Physics*, Vol. 131, pp. 267–279.

Bassi, F. and Rebay, S., 1997b. "High-order accurate discontinuous finite element solution of the 2D Euler equations". *Journal of Computational Physics*, Vol. 138, No. 2, pp. 251–285.

Buhmann, M.D., 1993. "New developments in the theory of radial basis function interpolation". *Multivariate Approximation: From CAGD to Wavelets, K. Jetter and FI Utreras, eds., World Scientific (Singapore)*, pp. 35–75.

Gao, H., Wang, Z. and Liu, Y., 2010. "A study of curved boundary representations for 2d high order euler solvers". *Journal of Scientific Computing*, Vol. 44, No. 3, pp. 323–336.

Luo, X.J., Shephard, M.S., O'bara, R.M., Nastasia, R. and Beall, M.W., 2004. "Automatic p-version mesh generation for curved domains". *Engineering with Computers*, Vol. 20, No. 3, pp. 273–285.

May, G. and Jameson, A., 2006. "A spectral difference method for the Euler and Navier-Stokes equations on unstructured meshes". In AIAA Paper No. 2006-0304, *Proceedings of the 44th AIAA Aerospace Sciences Meeting*. Reno, NV.

Moreira, F.M., , Breviglieri, E.J.C. and Azevedo, J.L.F., 2015. "High-order compressible flows simulations with the unstructured spectral difference method". In AIAA Paper No. 2015-3195*, Proceedings of the 22nd AIAA Computational Fluid Dynamics Conference*. Dallas, TX.

Moreira, F.M., Breviglieri, E.J.C., Aguiar, A.R.B. and Azevedo, J.L.F., 2016. "Implicit spectral difference method solutions of compressible flows considering high-order meshes". In AIAA Paper No. 2016-3352*, Proceedings of the 46th AIAA Fluid Dynamics Conference*. Washington, D.C.

Peiró, A.G., Roca, X., Peraire, J. and Sarrate, J., 2013. "High-order generation on CAD geometries". In *Proceedings of the VI International Conference on Adaptive Modeling and Simulation*. Lisbon, Portugal.

Persson, P.O. and Peraire, J., 2009. "Curved mesh generation and mesh refinement using lagrangian solid mechanics". In *47th AIAA Aerospace Sciences Meeting including The New Horizons Forum and Aerospace Exposition*. p. 949.

Rendall, T. and Allen, C., 2008. "Unified fluid–structure interpolation and mesh motion using radial basis functions". *International Journal for Numerical Methods in Engineering*, Vol. 74, No. 10, pp. 1519–1559.

Sherwin, S. and Peiró, J., 2002. "Mesh generation in curvilinear domains using high-order elements". *International Journal for Numerical Methods in Engineering*, Vol. 53, No. 1, pp. 207–223.

Wang, Z.J., Cagnone, J.S., Careni, D., de Wiart, C.C., Couaillier, V., Fidkowski, C., Galbraith, M., Hartman, R., Gooch, C.O., Persson, P.O., Hillewaert, K., Ekaterinaris, J., Huynh, H.T., Kroll, N. and Vincent, P., 2015. "HiOCFD4 4th international workshop on high-order cfd methods". `https://how4.cenaero.be`.

Wang, Z.J., Fidkowski, K., Abgrall, R., Bassi, F., Caraeni, D., Cary, A., Deconinck, H., Hartmann, R., Hillewaert, K., Huynh, H.T., Kroll, N., May, G., Persson, P., van Leer, B. and Visbal, M., 2013. "High-order CFD methods: Current status and perspective". *International Journal for Numerical Methods in Fluids*, Vol. 72, No. 8, pp. 811–845.

Wang, Z.J. and Liu, Y., 2002. "Spectral (finite) volume method for conservation laws on unstructured grids ii: Extension to two-dimensional scalar equation". *Journal of Computational Physics*, Vol. 179, No. 2, pp. 665–698.

Wang, Z.J., Liu, Y., May, G. and Jameson, A., 2007. "Spectral difference method for unstructured grids II: Extension to the Euler equations". *Journal of Scientific Computing*, Vol. 32, No. 1, pp. 3938–3956.

9 RESPONSIBILITY NOTICE

The authors are solely responsible for the printed material included in this paper.